presented at the ANSYS Convergence Conference, Houston 2015
Source: www.dynardo.de/en/library

Dynardo Technology and Applications to Well Completion Optimization for Unconventionals

Johannes Will[*1] and Taixu Bai[*2]

Stefan Eckardt[1], Dahai Chang[2], Ed Lake[2]

Abstract

The success of an unconventional hydrocarbon development depends on the effective stimulation of reservoir rocks. Industry practice is to conduct a large number of field trials requiring high capital investment and long cycle-time. The workflow and toolkits outlined in this paper offers a cheaper and faster alternative approach to optimizing the completion design for EUR (Estimated Ultimate Recovery) improvement.

The approach incorporates subsurface impacts to well stimulation design by employing subsurface parameters, and utilizes well diagnostic and well performance data to calibrate and constrain the models. It integrates subsurface characteristics, well, completion, operation, diagnostic, and well performance analysis. Using asset specific data, it is able to develop an optimal completion design with a set of prioritized completion and operation parameters. This results in reducing the number of field trials for achieving the optimal completion design. In addition, it provides valuable insights for further data acquisition to evaluate and forecast well performance.

Field trials based on the results from this approach have yielded encouraging production uplifts with quality forecasts. We believe it is technically feasible to derive an optimal completion design using a subsurface based forward modeling approach that will deliver significant value to the industry.

Introduction

Unconventional reservoirs produce substantial quantities of oil and gas. These reservoirs are usually characterized by ultra-low matrix permeability. Most unconventional reservoirs are hydraulically fractured in order to establish more effective flow from the reservoir and fracture networks to the wellbores. The success of hydraulic fracture stimulation in horizontal wells has the potential to dramatically change the oil and gas production landscape across the globe and the impacts will endure for decades to come.

For a given field development project, the economics are highly dependent completion establishing effective and retained contact with the hydrocarbon bearing rocks. Well and completion design parameters that influence the economic success of the field development include well orientation and landing zone, stage spacing and perforation cluster spacing, fluid volume, viscosity and pumping rate, and proppant volume, size and ramping schedule. Optimization of these design parameters to maximize asset economic value is key to the success of every unconventional asset.

[*]Corresponding authors. [1]Dynardo GmbH. [2]Shell Exploration and Production Company.

To achieve an optimal completion design for an asset, the current industry practice is to conduct a large number of field trials that require high capital investment and long cycle-time, and most importantly, significantly erode the project value. The workflow and toolkits shown in this paper are based on the Dynardo technology (Dynardo GmbH 2013) that offer a much cheaper and faster alternative approach in which to develop an optimal well completion design for EUR and unit development cost (UDC) improvements. It provides an integrated well placement and completion design optimization process that integrates geomechanics descriptions, formation characterizations, flow dynamics, microseismic event catalogues, hydraulic fracturing monitoring data, well completion and operational parameters in a modeling environment with optimization capability. The model is built upon a 3D geological model with multi-disciplinary inputs including formation properties, in-situ stresses, natural fracture descriptions, and well and completion parameters (i.e., well orientation, landing interval, fluid rate and volume, perforation spacing, and stage spacing). Upon calibrating with the hydraulic fracturing diagnosis data, the model provides optimized well completion design, and guidance on data acquisition and diagnostic needs to achieve EUR performance at optimized costs.

Field trials based on recommendations from the approach have yielded encouraging production uplift and have led to a significant reduction in the number of trials and cost compared to the commonly used trial-and-error approach. We believe it is technically feasible to derive an optimal completion design using a subsurface based forward modeling approach which will deliver significant value to the industry.

Dynardo Technology for Well Completion Optimization of Unconventional Reservoirs

The Dynardo technology [3] consists of a process to model, calibrate, and optimize well and hydraulic fracture stimulation designs for unconventional reservoirs using a novel approach developed at Dynardo GmbH. The technology combines three commercial software packages, ANSYS® (ANSYS, Inc. , 2013), multiPlas (Dynardo GmbH, 2013), and optiSLang® (Dynardo GmbH, 2013). The first module, ANSYS, is used as the solver for the parametric finite element modeling (FEM) of hydraulic fracturing processes in unconventional rocks (Fig. 1). The model construction and the execution are controlled by scripts (macros) developed by Dynardo using the ANSYS Parametric Design Language (APDL). The second module, multiPlas, is an ANSYS extension for non-linear material modeling of naturally fractured rocks developed by Dynardo. APDL programming also provides an anisotropic hydraulic element which models effectively the flow through fractured rock. The third module, optiSLang, is used to automatically calibrate the model and to perform sensitivity analyses with consideration of uncertainties in subsurface, completion design, and operational parameters. The Dynardo hydraulic fracturing workflow consists of a few key steps (Figure 2). They are parametric model construction, initialization, model execution and calibration, sensitivity study, and completion design optimization. All the steps are defined and executed automatically through optiSLang.

Model Construction and Initialization

The Dynardo hydraulic fracturing simulation workflow (Figure 1) starts with model construction based on input data. The required data is listed in Table 1, which covers inputs from multiple disciplines including geology, petrophysics, well, completion, production, and diagnosis. A sequential coupled hydraulic-mechanical modeling approach is applied in modeling the hydraulic fracturing processes. Therefore, two models, a hydraulic flow model and a mechanical model, are constructed simultaneously.

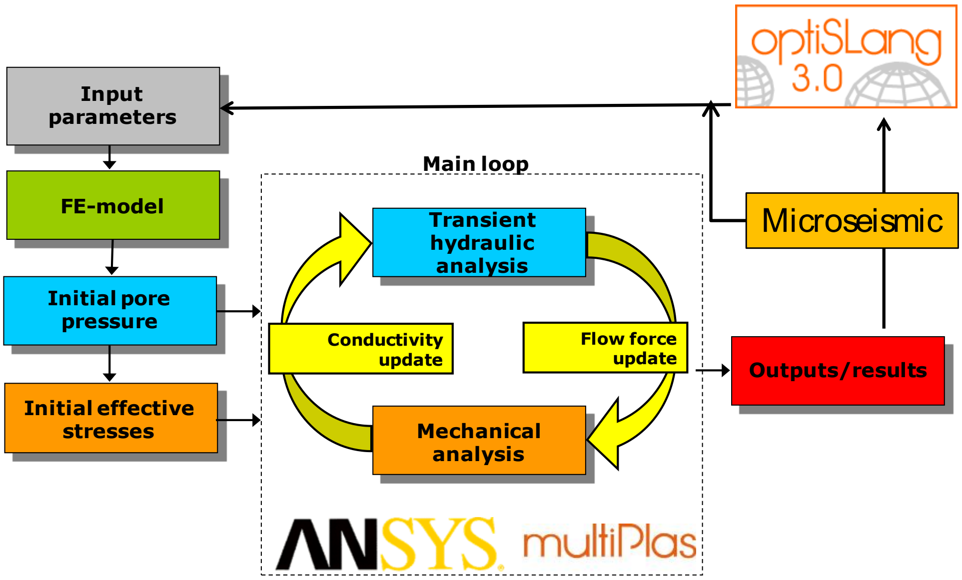

Figure 1: Schematics of key modules of Dynardo technology for hydraulic fracturing simulation and completion optimization.

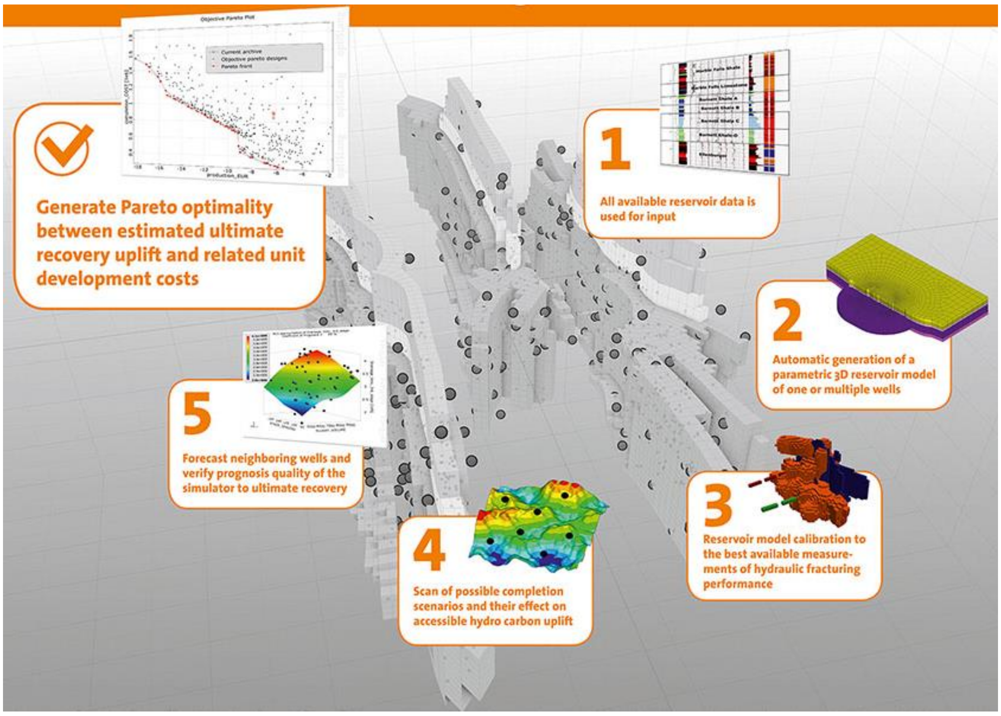

Figure 2: Dynardo workflow for hydraulic fracturing simulation and completion optimization.

Table 1: Required data and parameters for Dynardo hydraulic fracturing simulation and well completion optimization.

Geology	Petrophysics	Well & Completion	Geomechanics	Monitoring	EUR & Cost
Stratigraphic column	Porosity & permeability	Well survey data Stage spacing	In situ stresses Elastic properties	Microseismic PLT/DTs/DAS	EUR from RE

Layering & lithology Attitudes of beddings Natural fracture data	**Formation pressure Hydrocarbon saturation**	**Perforation cluster spacing Pumping pressure (or BHP) Pumping rate DFIT or mini-/micro-frac**	**Strength parameters of intact rocks Strength parameters of natural fractures**	**Tracer & isotope**	**Drilling cost Completion cost Market prices**

The model geometry considers layering of the reservoir formations. The layering is derived from geologic setting, well logs, and core measurement data with a balanced view of rock mechanical properties and reservoir properties. The key considerations include in situ stress, rock strength, natural fractures, and hydrocarbon contents in the layers.

In the models, only brick elements are used. The hydraulic flow model mesh is 8 times finer (i.e. a single mechanical element volume is presented by 8 hydraulic elements at 2 x 2 x 2) to sufficiently capture the pressure gradients in the process of fracturing. Elements with high aspect ratios are avoided. Domains of fine-mesh and coarse-mesh are defined in the parametric model to balance accuracy and computation efficiency. The size of fine mesh domain is chosen to ensure all microseismic events are included in the domain.

After model construction, the in-situ conditions are applied. In the hydraulic flow model, the pore-pressure field is initialized with the initial formation pressure. The mechanical model is initialized with the initial effective stress distribution. A non-linear mechanical analysis is performed to ensure consistency between the mechanical parameters and the initial stress fields, i.e., the rocks do not fail based on the failure criteria and the initial conditions and result in any plastic strains in the model.

Modeling Approaches

After model initialization, the actual simulation for hydraulic fracturing starts. A few details of the simulation are introduced below.

Homogenized Medium Approach

Hydraulic fracturing in unconventional shale reservoirs is dominated by stress and strength anisotropies of the reservoir rocks. The inherent anisotropies of shale reservoirs result from layering, deformation history, strength and stress variability, and non-uniform and anisotropic conductivity of the fractured rock mass. To capture the anisotropic nature of the reservoir rocks and its impact on hydraulic fracturing, we believe three-dimensional modeling of anisotropic strength, stress, and conductivity of rock matrix and fracture system is required. Simulation simplification to 2D or pseudo-3D models may fail to capture the effects necessary to properly model some important effects, which may drive the hydraulic fracturing process and the resulting production performance, and may fail to identify the opportunities for economics and production improvements (Weijers, October 2007).

Most shale hydrocarbon resources are naturally fractured or have planes of weakness. Full-3D modeling of multiple stages and multiple wells in a complex reservoir setting is achievable either with a discrete modeling approach of natural fractures or a homogenized modeling approach. However, the discrete modeling approach is currently computationally too expensive to be practical for the scale of the multi-stage multi-well problems. Although a majority of research groups are following discrete fracture modeling approaches, a full-3D discrete solution appears elusive at the needed problem scale. Therefore, the Dynardo technology uses a homogenized continuum approach to model the 3D hydraulic fracturing in naturally fractured reservoirs. This is to improve numerical efficiency and, in the meantime, to capture the necessary physical and mechanical processes in full-3D modeling of hydraulic fracturing of multiple stages and multiple wells in unconventional reservoirs.

The homogenized continuum approach was initially developed and applied in the Civil Engineering fields of waterway and dam engineering to better determine the influence of water flow in naturally fractured dam foundations (Wittke, 1984). It was successfully implemented for academic and industrial applications by Wittke [5] and others in the 1980s and 1990s.

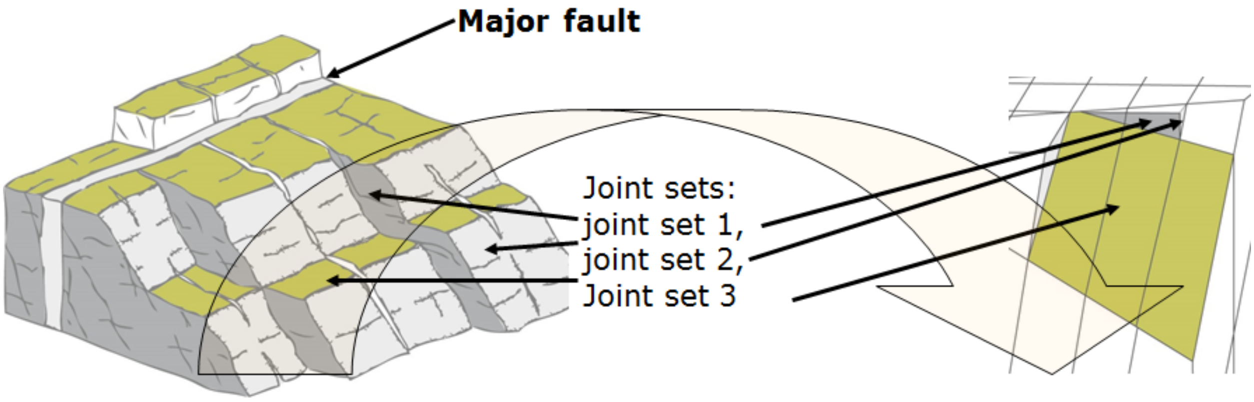

Figure 3: Naturally fractured (jointed) rocks treated as homogenized continuum.

In the homogenized continuum approach, the rocks are treated as having isotropic "intact" rock strength with multiple sets of planes of weaknesses. In this paper, these planes of weaknesses include natural fractures, which are usually grouped as "fracture sets or joint sets" (Figure 3, joint set 1&2) based on their orientations and cross-cutting relationships, and bedding planes (Figure 3, joint set 3). Although the natural fractures and bedding planes are not explicitly modeled as discrete features, their influences are explicitly accounted for with anisotropic strength models of fractured rocks. The anisotropic strength models lead to anisotropic conductivity development in hydraulic fracturing processes. When a fracture or bedding plane opens or dilates, the associated conductivity increases due to either an oriented tensile or an oriented shear failure. After pumping stops, fracture aperture reduces because of net pressure decline. Consequently, the associated fracture conductivity reduces. Both of these effects are taken into account in the Dynardo model.

In the simulation, the tensile and shear failure modes of intact rock and of the natural fractures are consistently treated within the framework of multi-surface plasticity [9]. The multi-surface strength criterion is evaluated at every discretization point in space. If the stress state violates the multi-surface yield criterion, then plastic strains develop and strength degradation occurs. By introducing "mean effective" activated fracture spacing, which can be defined for each set of natural fractures and for each individual layer, the fracture opening and the corresponding fracture conductivity can be calculated based on the plastic strain.

Sequentially-Coupled Hydraulic Flow-Mechanical Modeling

Hydraulic fracturing is a coupled hydraulic flow-mechanical problem. In the hydraulic flow model, pressure increases in the fracture initiation locations due to the pumping of fluid and low rock matrix permeability. With the homogenized continuum approach, pressure is treated as the pressure in the fractured rock. Mechanically, pressure increase changes the effective stresses within the rock. If the pressure is large enough, the rock starts to fail and fractures open. As a result, the permeability of the fractured rock increases that changes the pressure distribution in the hydraulic flow model. The coupling between the models is realized by updates of material parameters and loading conditions in the hydraulic flow and mechanical models.

The coupling is performed in an explicit way (Figure 4). Consequently, one iteration cycle is performed for every time step. The time step needs to adequately represent the progress of the fracture growth. At each time step, a transient hydraulic flow analysis starts first. Then the mechanical analysis with the updated pressure field from the hydraulic flow model is conducted. The mechanical analysis results in new stress and plastic strain fields and updated hydraulic conductivities. The updated hydraulic conductivities are applied to the hydraulic model in the subsequent time step. Because of the anisotropic nature of fractured rock conductivity, anisotropic conductivity tensor is used in the calculation.

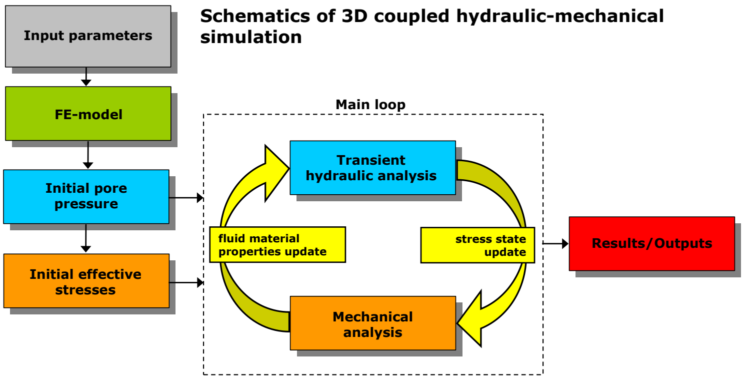

Figure 4: Schematics of hydraulic flow-mechanical coupling.

Non-Linear Mechanical Analysis

In the mechanical model, a nonlinear static finite element analysis (Bathe, 1985) is performed. The nonlinearities are caused by failure of the material. The nonlinear constitutive behavior of fractured rock is described with the external library multiPlas (Dynardo GmbH, 2013) that contains user-defined nonlinear material models for typical materials in geomechanical and civil engineering studies.

The mechanical analysis of fractured rock incorporates the concept of effective stresses. The effective stress tensor $\boldsymbol{\sigma_{eff}}$ is defined as:

$$\boldsymbol{\sigma_{eff}} = \boldsymbol{\sigma_{tot}} + p\boldsymbol{I}, \tag{1}$$

where $\boldsymbol{\sigma_{tot}}$ is the total stress tensor, p is the pressure and $\boldsymbol{I}$ is the second order identity tensor. Note, that compressive stresses are negative.

The homogenized continuum approach is applied to describe the deformation behavior of fractured rock. Consequently, the stress-strain relationship does not describe the deformation behavior of the individual constituents, i.e., intact rock and fractures, but the overall response of the homogenized fractured rock mass. The corresponding linear-elastic stress strain relationship can be written as:

$$\boldsymbol{\sigma}_{eff} = \boldsymbol{D} : \boldsymbol{\varepsilon}, \tag{2}$$

where $\boldsymbol{D}$ is the orthotropic linear elastic material tensor of the homogenized rock mass and $\boldsymbol{\varepsilon}$ is the strain tensor.

In multiPlas, the description of the nonlinear behavior of fractured rock is based on the concept of rate-independent plasticity (Simo & Hughes, 1998) (Jirasek & Bazant, 2001). It is assumed that the total strain $\boldsymbol{\varepsilon}^{tot}$ can be decomposed into an elastic part $\boldsymbol{\varepsilon}^{el}$ and a plastic part $\boldsymbol{\varepsilon}^{pl}$:

$$\boldsymbol{\varepsilon}^{tot} = \boldsymbol{\varepsilon}^{el} + \boldsymbol{\varepsilon}^{pl}. \tag{3}$$

The stresses are related to the elastic strains by the linear elastic material matrix. Consequently, Eq. (2) can be rewritten as:

$$\boldsymbol{\sigma}_{eff} = \boldsymbol{D} : \boldsymbol{\varepsilon}^{el}. \tag{4}$$

The plastic strains develop if a certain strength criterion, conventionally referred to as the yield condition, is violated. In this context, the boundary of the admissible stress space (elastic domain) is called yield surface.

The strength of the homogenized fractured rock is defined by the strength of the individual constituents. As a result, the overall strength criterion is not a smooth surface, but is composed of multiple yield surfaces. Each yield surface represents a specific failure mode of one of the constituents. In the multiPlas material model for fractured rock, isotropic strength is assumed for intact rock (Figure 5). Two fundamental failure modes are considered. Tensile failure of intact rock is represented by the Rankine yield surface. The corresponding yield condition can be written as:

$$F_{RK,I} = \sigma_1 - f_{t,I} \leq 0, \tag{5}$$

where σ_1 is the maximum effective principal stress (tensile stresses are positive) and $f_{t,I}$ is the uniaxial tensile strength. Shear failure of intact rock is described by the Mohr-Coulomb yield condition, which reads:

$$F_{MC,I} = \frac{\sigma_1 - \sigma_3}{2} + \frac{\sigma_1 + \sigma_3}{2} \sin \varphi_I - c_I \cos \varphi_I \leq 0, \tag{6}$$

where φ_I is the intact rock friction angle, c_I the cohesion, σ_1 is the maximum effective principal stress, and σ_3 is the minimum effective principal stress.

The multiPlas material model currently allows defining up to four natural fracture sets. Unlike intact rock, the strengths of natural fractures are anisotropic. The strength criteria depend on the orientation of the natural fracture set, which is described by the dip direction α and dip angle β. The corresponding yield surfaces are defined in terms of the normal stress $\sigma_{N,J}$ and the in-plane shear stress τ_J. Both stress components are obtained by rotating the global stress tensor into the local coordinate system associated with the set of natural fractures. Similar to intact rock, two failure modes (Figure 5) are taken into account for every fracture set. The tension cut-off yield surface represents tensile failure normal to the fracture. The corresponding yield criterion reads:

$$F_{T,J} = \sigma_N - f_{t,J} \leq 0, \tag{7}$$

where $f_{t,J}$ is the tensile strength of the fracture set. Shear failure of natural fractures is described by the Mohr-Coulomb yield surface:

$$F_{MC,J} = \tau_J + \sigma_N \tan\varphi_J - c_J \leq 0, \tag{8}$$

where φ_J is the friction angle and c_J is the cohesion of the set of natural fractures.

The yield surfaces of the multiPlas fractured rock material model are visualized in Fig. 5. In the simulation, when a strength criterion is met, the corresponding strength parameters are reduced to residual values. Dilation effects are taken into account for shear failure by incorporating non-associated flow rules. The corresponding plastic potentials are obtained from the Mohr-Coulomb conditions by replacing the friction angle with the dilation angle in Eqs.(6) and (8).

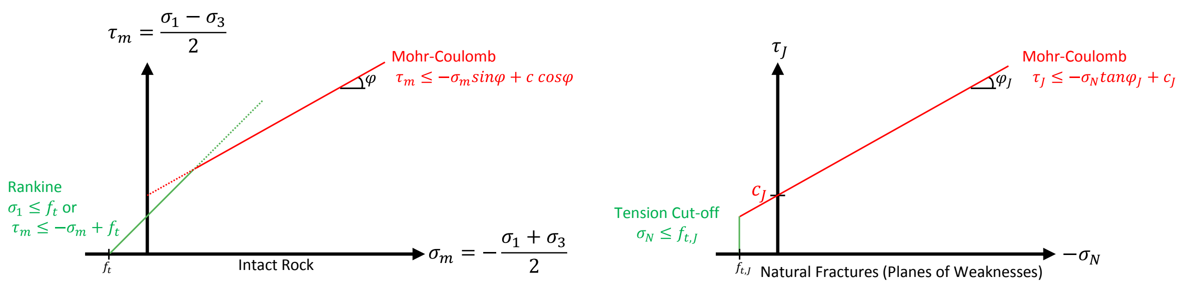

Figure 5: Yield surfaces of intact rock and nature fractures (planes of weaknesses) in multiPlas.

Numerical Treatment of Multiple Strength Conditions

The non-linear behavior of fractured rock is described by a set of different strength conditions. As a result, the boundary of the admissible stress space becomes non-smooth requiring a special numerical treatment. In multiPlas, the multi-surface plasticity approach, introduced by (Simo & Hughes, 1998), is implemented and allows for an efficient and consistent treatment of multiple yield conditions.

In the multi-surface plasticity approach, the plastic strain increment is defined by a modified flow rule which can be written as:

$$\boldsymbol{\Delta\varepsilon^{pl}} = \sum_{\alpha=1}^{n_{YC}} \Delta\lambda^\alpha \boldsymbol{g^\alpha}, \tag{9}$$

where n_{YC} is the number of yield conditions, $\Delta\lambda^\alpha$ is the plastic multiplier, and $\boldsymbol{g^\alpha}$ is the direction of plastic flow of yield condition α. A stress state is admissible if all yield conditions are satisfied. If the stress state is on a yield surface, then plastic strains develop for that yield surface. Because the flow rule defines an oriented direction of plastic flow, the corresponding plastic multiplier must be positive. Every stress state needs to satisfy the conditions known as Kuhn-Tucker form of loading and unloading conditions for each yield criterion:

$$F_\alpha \leq 0,\ F_\alpha \Delta\lambda^\alpha = 0, \text{ and } \Delta\lambda^\alpha \geq 0, \text{ for } \alpha = 1 \ldots n_{YC}. \tag{10}$$

Consequently, in a plastic step, the stress state might be located on more than one yield surface. This is illustrated in Figure 6 for a two surface model. In order to handle the singularity at the intersection between both yield surfaces, the stress state must satisfy both conditions. As a result, the direction of plastic strain is defined as a combination of the individual directions.

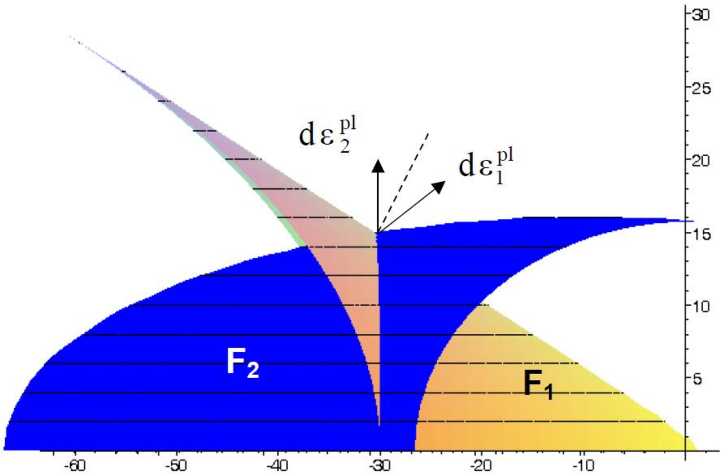

Figure 6: Intersection between the two flow criteria F1 and F2.

In the numerical implementation, the stress-calculation is performed in two steps. In the first step, a trial stress state is calculated assuming that the plastic strain obtained in the previous step does not change. The yield conditions are evaluated for this trial stress state. A set of active yield surfaces are defined by all yield conditions that are violated by the trial stress state. If no yield condition is violated, the trial stress state is admissible. Otherwise, the trial stress needs to be returned to all active yield surfaces. In this second step, the standard return mapping algorithms, i.e., cutting plane or closest point projection, are applied. In contrast to the classical single-surface plasticity, the return mapping algorithm must simultaneously handle multiple yield surfaces that result in a system of nonlinear equations. A yield condition is removed from the set of active yield surfaces if the corresponding plastic multiplier becomes negative during the iteration.

Hydraulic Flow Analysis

In the hydraulic step, a transient analysis is performed. In order to cover gravity effects, the governing equations are not expressed in terms of pressure, but rather in terms of hydraulic head. The hydraulic head h of a fluid is defined as the combination of the pressure head and the elevation head:

$$h = \frac{p}{\rho\, g} + z, \tag{11}$$

where p is the pressure, ρ is the fluid density, g is the standard gravity, and z is the elevation.

The analysis is based on the groundwater flow equation:

$$S_s \frac{\partial h}{\partial t} = -\nabla \boldsymbol{q} + R, \tag{12}$$

where S_s is the specific storage, R is a general source and sink term, and $\boldsymbol{q}$ is the flux vector. The specific storativity is one of the most important hydraulic parameters that needs to be calibrated for the reservoir. The storativity represents the amount of stored energy in open fractures and is related to the energy losses due to friction or leak-off during the hydraulic fracturing process.

Similar to the mechanical model, the continuum theory is applied in the hydraulic model. As a result the flux vector can be related to the hydraulic head by Darcy's law:

$$\boldsymbol{q} = -\boldsymbol{K}\,\nabla h\,, \tag{13}$$

where $\boldsymbol{K}$ is the conductivity matrix of the fractured rock.

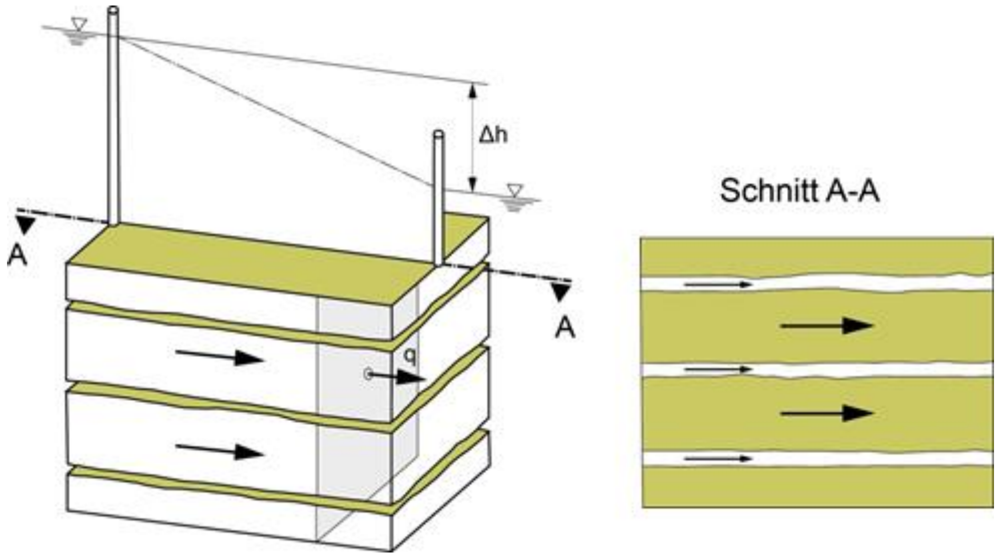

Figure 7: Fluid flow in homogenized fractured media.

As shown in Figure 7, the Darcy equation describes the flow through the homogenized fractured rock. The hydraulic conductivity matrix $\boldsymbol{K}$ represents the overall conductivity of the rock including the fractures. The homogenized conductivity is obtained by superimposing the contributions of the individual constituents:

$$\boldsymbol{K} = \boldsymbol{K_I} + \sum_{j=1}^{n_{JS}} \boldsymbol{K_J^{(j)}}, \tag{14}$$

where $\mathbf{K_I}$ is the hydraulic conductivity of intact rock, $\mathrm{n_{JS}}$ is the number of fracture sets, and $\mathrm{K_J}$ is the hydraulic conductivity of the fracture set *J*. The intact rock conductivity represents the initial rock conductivity. By assuming a transversely isotropic behavior, the intact rock conductivity matrix is given by:

$$\boldsymbol{K_I} = \frac{\rho\, g}{\mu}\begin{bmatrix} k_{ini,h} & 0 & 0 \\ 0 & k_{ini,h} & 0 \\ 0 & 0 & k_{ini,v} \end{bmatrix}, \tag{15}$$

where ρ is the fluid density, g is the standard gravity, μ is the dynamic fluid viscosity, $k_{ini,h}$ is the matrix permeability of the rock parallel to the bedding, and $k_{ini,v}$ is the matrix permeability of the rock perpendicular to the bedding. Failure of intact rock does not change the rock matrix conductivity. Intact rock failure is handled by introducing additional fracture sets. In the local coordinate system of the fracture set, the fracture conductivity matrix is given by:

$$\boldsymbol{K_J'} = \frac{\rho\, g}{\mu} k_J \begin{bmatrix} 1 & 0 & 0 \\ 0 & 1 & 0 \\ 0 & 0 & 0 \end{bmatrix}, \tag{16}$$

where k_J is the in-plane fracture permeability. In the initial state the fracture permeability is zero. If a natural fracture set fails, the fractures open up and the fracture permeability increases.

The global fracture conductivity matrix is obtained by rotation of the local matrix:

$$\boldsymbol{K_J} = \boldsymbol{R}^T \boldsymbol{K}_J' \boldsymbol{R}, \tag{17}$$

where $\boldsymbol{R}$ is a matrix describing the rotation from the global into the local coordinate system of the fracture set. In the global coordinate system, the fracture conductivity matrix is generally anisotropic. As a result, the homogenized conductivity matrix $\boldsymbol{K}$ becomes anisotropic in the simulation.

By substituting Eq. 13 into Eq. 12, the transient seepage equation is obtained:

$$S_s \frac{\partial h}{\partial t} = -\nabla(\boldsymbol{K}\, \nabla h) + R, \tag{18}$$

This equation is solved using finite element techniques.

Calculating fracture opening and fracture conductivity

In the mechanical analysis, the development of fractures is represented by a plastic material model. As a result, fracture opening is not directly measured but needs to be calculated based on the plastic strains. Additional history variables are introduced which monitor the normal plastic strains of every fracture set during the mechanical analysis. Both failure modes, tensile and shear, result in a normal plastic strain component. The amount of normal plastic strain due to shear failure can be controlled by the dilation angle. For a specific fracture set, the normal plastic strain increases only if the corresponding yield surfaces are active. The mechanical (geometrical) fracture opening of a fracture set E is defined as:

$$E = \varepsilon_N^{Pl}\, S, \tag{20}$$

where ε_N^{Pl} is the plastic strain normal to the fracture and S is the average activated fracture spacing. The activated fracture spacing is an input parameter and needs to be calibrated. If the activated fracture spacing becomes larger than the element size, in order that the continuum theory remains valid, the activated fracture spacing is limited by an equivalent element length l_{eq}:

$$S \leq l_{eq}, \tag{21}$$

The equivalent element length is a one-dimensional measure for the size of the domain represented by an integration (material) point. According to Reference (Pölling, 2000), the equivalent element length l_{eq} for an 8-node brick element with 8 integration points can be defined as:

$$l_{eq} = \sqrt[3]{\frac{V_e}{8}}, \tag{22}$$

where V_e is the element volume.

In the derivation of fracture permeability in Reference (Wittke, 1984), a laminar flow between two smooth planes is assumed. In reality, the fracture surface is neither planar nor smooth. Consequently, the mechanical opening must be related to the effective hydraulic opening of the idealized fracture (Barton, Bandis, & Bakhtar, 1985) (Iragorre, 2010). The following relationship is applied:

$$e = \frac{E}{r_{Ee}}, \tag{23}$$

where e is the effective hydraulic opening and r_{Ee} is a prescribed ratio of mechanical fracture opening to effective hydraulic opening. In most applications, a ratio between 1 and 2 is used initially, and later adjusted and verified during the calibration process.

The relationship between the effective hydraulic opening and the hydraulic fracture permeability is given by the cubic law:

$$k_J = \frac{e^3}{12\, S\, R_C}, \tag{24}$$

where R_C is the fracture roughness coefficient. This relationship is visualized in Fig. 8. In order to be able to limit the flow in the fracture, a maximum effective hydraulic opening, e_{max}, is introduced. This maximum hydraulic opening results in the maximum hydraulic conductivity, and is related to the in-situ stress, the fluid, and the proppant placement condition. A limitation to this value can usually be seen in experimental data. This parameter is one of the most important model parameters and should be properly calibrated.

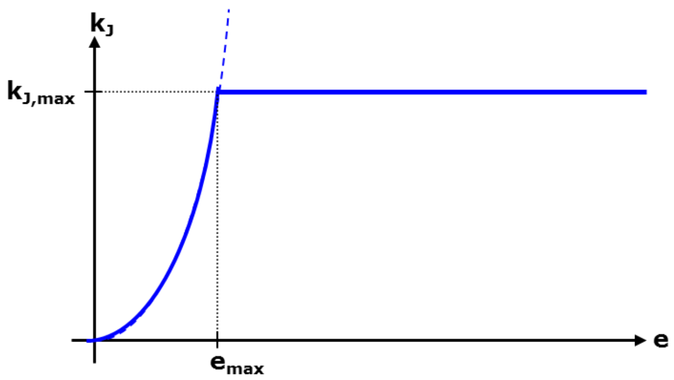

Figure 8: Relation between fracture permeability and fracture opening.

Stress Dependent Fracture Openings

Since the fracture opening is described by a plasticity model, the closure of fractures, i.e., the reduction of normal plastic strains, is not represented in the mechanical model. The effect of normal stresses on fracture permeability is not taken directly into account in Eq. 24. As shown in Reference (Iragorre, 2010), this effect can be observed in experiments and will have a significant influence on the resulting fracture conductivity during production. The Dynardo technology optionally allows for this effect to be managed. If the stress dependency is enabled, then the fracture permeability is calculated as:

$$k_J(e, \sigma_N) = f(\sigma_N) k_{J0}(e), \tag{25}$$

where k_{J0} is the stress independent fracture permeability given by Eq. 24, f is a dimensionless scaling factor ranging from a minimum value to 1, and σ_N is the normal stress. Based on (Gangi, 1978) the following stress dependency function is implemented:

$$f(\sigma_N) = \begin{cases} 1 & \sigma_N > 0 \\ (1 - f_{min}) \left[1 - \left(\frac{\sigma_N}{D}\right)^{\frac{1}{n}}\right]^2 + f_{min} & D \leq \sigma_N \leq 0, \\ f_{min} & \sigma_N < D \end{cases} \tag{26}$$

where D is the limit compressive stress (negative), f_{min} is the minimum scaling factor, and n is a shape factor. Figure 9 visualizes the influence of that shape factor. For the post-processing of the fracture openings, the openings are recalculated by introducing the stress dependent fracture permeability into the cubic law, Eq. 24.

The conductivity decline function (stress dependency function) is affected by the proppant placement in the fractures. In general, higher pressures are required to close a fracture that is filled with proppant than a fracture without proppant. This effect is taken into account by defining two different stress dependency functions, namely limit stress and minimum scaling factor. The stress dependency function for fractures with proppant is applied in all elements having proppant-accepting mechanical fracture openings and which are connected to perforation clusters with elements having all proppant-accepting fracture openings. In all other elements, the stress dependency function for fractures without proppant is used. Usually the stress dependency parameters are derived through lab testing of conductivity at varying proppant concentrations and normal stress conditions.

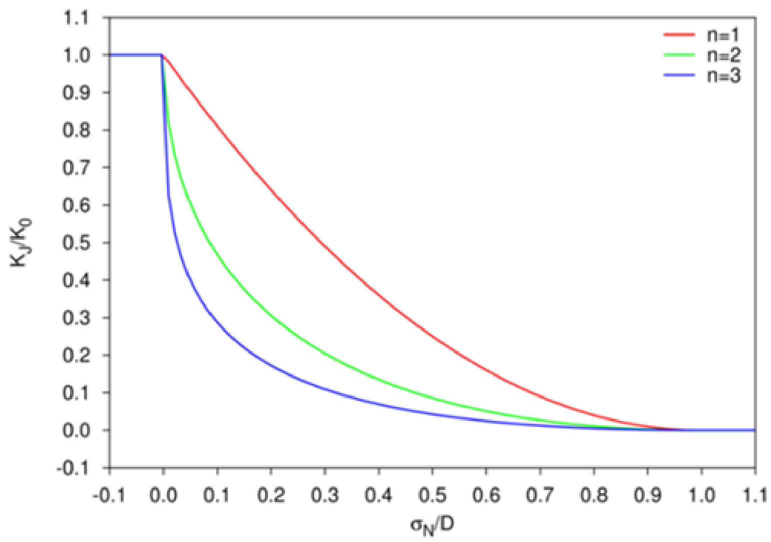

Figure 9: Stress dependent fracture conductivity.

Intact Rock Failure Effects on Hydraulic Conductivity Tensor

In addition to failure of natural fractures, the intact rock might fail as well, and the hydraulic conductivity of the fractured rock increases. In order to capture this phenomenon, up to three additional fracture sets, one for tensile failure and two for shear failure, are introduced in case of intact rock failure. These additional fracture sets are introduced if the corresponding intact rock failure criterion is violated for the first time. In the case of tensile failure where the Rankine yield surface becomes active, the additional fracture is oriented perpendicular to the maximum principal stress direction. In the case of shear failure where the Mohr-Coulomb yield surface becomes active, the orientation of two additional fracture sets coincides with the orientation of the shear failure planes in that step. After initialization of the additional fracture sets, the orientation is fixed for that element for the duration of the simulation. For these additional fracture sets, the fracture conductivity is calculated in the same way as for the pre-defined fracture sets.

Fluid Pressure Mapping to Mechanical Model

Fluid flow in fractures results in normal forces and shear forces at the fracture surfaces (Wittke, 1984). In the global coordinate system, the flow force vector $\boldsymbol{J_{ff}}$ acting on the element volume (body force) can be written as:

$$\boldsymbol{J_{ff}} = \rho\, g\, \boldsymbol{I}, \tag{27}$$

where ρ is the fluid density, g is the standard gravity, and $\boldsymbol{I}$ is the gradient of the hydraulic head. The corresponding nodal force vector is obtained by integration of the flow force vector over the element volume. The individual nodal contributions are assembled and transferred to the mechanical model. Because of the incremental solution procedure, only the variations of the flow forces are added to the nodal forces in the mechanical model at every time step.

Well and Perforation Flow Modeling

In the hydraulic model, the reservoir inclusive of the perforations is modeled by solid elements. Additional 1-D pipe elements are introduced to connect the perforations of one stage to the volume elements. Figure 10 shows the pipe definition in the model. The red line represents the wellbore which connects the perforations. The hydraulic properties of the wellbore are defined by its inner diameter and corresponding pipe conductivity. In general a large conductivity value is applied for the wellbore. The green lines are the equivalent perforation tunnels that connect the wellbore with the center of the reservoir volume elements. The perforation pipes are introduced to model a pressure drop between the well and the end of perforation. The hydraulic conductivity of the perforation pipes are defined in terms of a prescribed pressure drop relation:

$$K_{perf} = \frac{4\, \rho g\, L}{\pi\, d_{Perf}^2\, \Delta P} \frac{Q_{Ref}}{n_{Perf}}, \tag{28}$$

where L is the pipe length, d_{Perf} is the pipe diameter, Q_{Ref} is the reference slurry rate, and n_{Perf} is the number of perforations. The pipe elements are automatically created during the parametric model generation process.

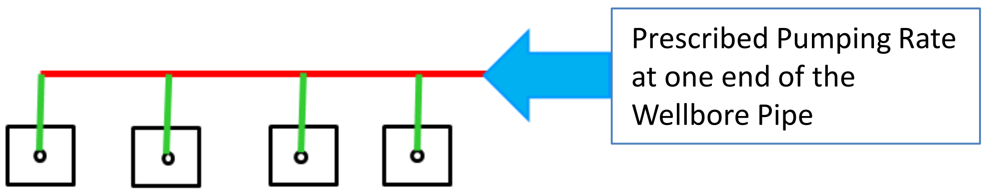

Figure 10: Pumping rate boundary condition.

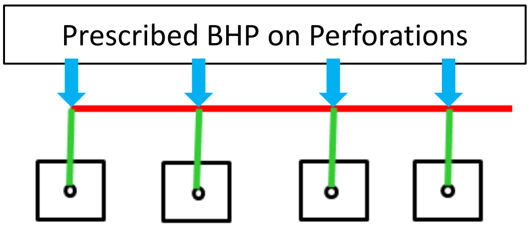

Figure 11: Bottom hole pressure boundary condition.

In the simulation, the loading conditions are applied either to the well pipe or to the perforation pipe. Two types of loading conditions are supported, i.e., flux and pressure.

A flux loading condition is defined by prescribing pumping rate. By applying the pumping rate to the well pipe, as shown in Figure 10, we mimic flow distribution among the perforations as in actual frac jobs. In other words, the flow through a perforation into the formation is determined by the resistance of fracture propagation at that perforation location.

Alternatively, a pressure loading condition can be applied by prescribing bottom-hole pressure (BHP). In this case, the measured or calculated BHP pressure is applied directly to the perforation pipe. Figure 11 shows that BHP is prescribed at the nodes at the intersections between perforation pipes and well pipe.

Model Calibration

After model construction, calibration of large amounts of uncertain parameters to the best available measurements is conducted. A parameter identification problem exists simply because of the large number (>100) of model parameters, and they may have a considerable associated uncertainly. During the calibration phase, Dynardo applies optiSLang [4], the Dynardo software for variation and optimization analysis. The process involves running a set of calibration models with respect to the variation space of the model. With optiSLang, important parameters in the parametric hydraulic fracture model can be identified and successively updated for successive model runs, are initialized and executed in an automated process. With that procedure a large number of calibration sensitivity design runs can be executed in a relatively short period of time.

The calibration phase ideally requires quality diagnostic data. This includes surface pressure, bottom hole pressure, and pumping rate histories from diagnostic fracture injection testing (DFIT), which are used to derive instantaneous shut-in pressure (ISIP), and the pressure and pumping rate histories and the total slurry volume (fluid plus proppant) for each stage of the actual frac job. The representative microseismic event catalog is also used in the calibration phase. With optiSLang reservoir uncertainties are integrated in the calibration process to better identify the most influential parameters controlling fracture geometry. Thus, model calibration process also provides insights for additional data gathering to focus on parameters that significantly affect the simulation results. The details of the calibrations are explained below.

Calibrating of Fracture Initiation and Termination Conditions

After model initialization with in-situ stress field and initial pressure conditions, the pressures at which hydraulic fractures initiation and termination are verified. ISIP from DFIT is used to define fracture initiation and fracture extension. Uncertainty of ISIP is estimated with minimum, mean, and maximum values. Typical adjustments during calibration to ISIP conditions include formation pressure and in-situ stress conditions within and nearby the perforated layers, and strengths of the natural fractures within and nearby the perforated layers.

Calibrations with Bottom Hole Pressure and Pumping Rate

By applying the actual pumping rate, we calculate the BHP (bottom hole pressure) response and compare with the measured BHP (or projected BHP from the surface pressure) based on data from the actual frac job. Conversely, by applying the BHP from the frac job, we calculate the flow rate through the perforations into the formation and compare the calculated value with the measured pumping rate. The major parameters calibrated in this step are strengths of intact rocks, activated mean spacings and strengths of the natural fractures in the different layers, maximum hydraulic opening of the activated fractures, and overall energy loss due to friction, leak off, turbulent flow or other dissipate mechanisms that are summed up into the specific storativity of the Darcy flow equation.

Calibration of Generated Fracture Volume with Pumped Total Fluid Volume

The generated fracture volume is compared with the pumped total fluid volume in the rate and pressure calibration introduced above. The generated total fracture volume is calculated based on mechanical openings of the fracture. As the permeability of unconventional rocks is low in general, and assuming very low fluid leak off during fracing, the total fracture volume should be close to the pumped total fluid volume. Since proppant placement is not explicitly modeled in the current approach, we count the proppant volume into the total fluid volume in this calibration.

Calibration of Computed SRV with Microseismic Data

Microseismic data provides the time, the position (point), and the magnitude of each individual microseismic event, which is believed to represent shear failure of reservoir rocks during hydraulic fracturing. The “dot-plot” of microseismic events is used as a representation of the spatial extension of hydraulic fractures. For model calibration with microseismic data, the “dot-plot” is compared to the simulated rock failure. In this context, two different methods are applied. In the first method, the microseismic events and calculated stimulated rock volume (SRV) represented by the collection of all failed elements are plotted together at different time steps. This allowed a visual comparison of spatial distribution of both of the data sets. The check point in this calibration is to see whether the SRV extensions from the model fit the overall hydraulic fracture length and height indicated by the microseismic data in the horizontal and vertical directions, respectively. The drawback of this method is that it is very challenging to define a clear objective measure for the quality of the fit, which is needed for in the automatic calibration procedure.

In the second method, the mechanically failed elements are considered as “cracking” events. If the calculated fracture opening in a failed element exceeds a certain threshold, the time step and the location of the element center point is stored. The distance between the center of the cracked element to the stage center is calculated. The calibration is to compare the distance with the distance between the microseismic event and the stage center.

Optimization of Well and Completion Designs

Once the model is calibrated with all the procedures described in the previous section, it is then used in forecast mode to optimize well and completion designs. The optimization involves two critical procedures, i.e., defining the objective function for optimization and defining the parametric space. Parametric modeling is conducted with respect to two parametric spaces. First is the subsurface parametric space, which represents the reservoir uncertainties and gives the ranking of subsurface parameters based on their impacts to the objective function. It provides insights to future data acquisition programs. The second are the well and completion parameters, which yield the optimized well and completion design corresponding to the objective function.

Most of the subsurface parameters are defined for each individual layer and for each natural fracture set in the model. Together with the well and completion parameters, it is common that several hundred parameters are defined. To handle this large amount of parameters and their uncertainties, the Dynardo technology utilizes optiSlang, which performs a few procedures including searching the whole uncertainty space defined by the uncertainty ranges of all the parameters as well as experimental design scenarios, generating ANSYS input files corresponding to the generated scenarios, launching ANSYS simulations with the input files, taking ANSYS analysis results from the simulations and saving the results in a database. After a certain sample set is completed optiSLang search for subspaces of important parameters and generates mapping functions between inputs and simulation result variations in the so called the metamodel. The metamodels are checked for their forecast quality based on their responses to input variations. After the forecast quality reaches certain levels such as 90% the sampling stops. The metamodels provide insights about the ranking of the parameters based on their impacts to the objective functions defined in the study.

Objective Functions

An objective function is defined based on the specific business driver for an asset. There are a few potential objective functions, including, but not limited to, total stimulated rock volume (TSRV), valuable SRV (VSRV), total drainage volume (TDV), accessible hydrocarbon initially in place (AHCIIP), EUR, and UDC.

TSRV is the total volume of all the mechanically failed elements in the model. It is a gross measure of the effectiveness of the fracture stimulation. Only a fraction of TSRV contributes significantly to production. To address the importance of SRV to production, two concepts are proposed, connected-water-accepting volume (CWAV) and connected-proppant-accepting volume (CPAV).

Based on the mechanical fracture openings, elements are identified as water-accepting or as proppant-accepting. An element is called a *water-accepting element* if the mechanical opening of at least one fracture set in the element exceeds a predefined threshold. Usually a threshold of 0.1 mm is applied. A *proppant-accepting element* is identified if the mechanical opening of at least one fracture set exceeds a multiple of the average proppant size. In most of the Dynardo simulations, a threshold of three times the average proppant size is applied.

In addition to the water-accepting and proppant-accepting elements, their connectivity to the perforations is identified. An element is *connected-water-accepting element* if the fluid can flow from any perforation directly into that element or through other water-accepting elements. The same principle is applied with to the definition of connected-proppant-accepting elements. The total volume of all connected-water-accepting elements is called the *connected-water-accepting volume* (CWAV). Similarly, the *connected-proppant-accepting volume* (CPAV) is defined.

The CWAV and CPAV are continuously updated during the simulation. At the beginning of the simulation, only the perforation elements are considered in the CWAV and CPAV. After every mechanical step, the water-accepting and proppant-accepting elements and their connectivity status are updated. Based on the connectivity status from the previous step, the neighbouring water-accepting or proppant-accepting elements are selected and added to the corresponding CWAV or CPAV. Two elements are neighbouring elements if they share at least one node. This selection algorithm is continued until no new neighbour elements are found.

For CPAV, successful proppant placement is assumed. Proppant effects are captured in the fracture conductivity decline function. The stress dependent fracture conductivity decline with proppant is only used for the CPAV. Otherwise the stress dependent conductivity decline without proppant is applied even if the fracture opening is greater than the proppant-accepting opening threshold.

It is observed that only the CPAV is valuable to the production, especially in relatively soft rocks. Therefore, CPAV is equivalent to VSRV. VSRV is defined as total volume of elements with fracture opening greater than three times of predefined proppant size and with connection, direct or indirect through other proppant-accepting elements, to at least one perforation cluster.

TDV is defined as the total volume of all elements that can be drained during the production time of the well through the VSRV. The VSRV is part of the drainage volume by this definition. An element outside of the VSRV in the drainage volume is based on the criteria that the element is in the same element layer of the layered reservoir with at least one connected-proppant-accepting element, and the distance between the element center and the center of the nearest proppant-accepting element is less than the *drainage distance*, which is given by an empirical relation in the form of:

$$R\,[ft] = C\sqrt{k_{ini,h}\,[nD]}, \tag{29}$$

where *C* is a constant, $k_{ini,h}$ is the matrix horizontal permeability of the rocks in the layer.

The criteria are defined with consideration of the permeability anisotropy of unconventional rocks, i.e., the horizontal permeability of the rocks is usually several orders of magnitude larger than the vertical permeability due to layering and the laminated natural of unconventional rocks.

ACHIIP is estimated based on TDV and hydrocarbon content, which can be calculated with:

$$AHCIIP = \sum_{i=1}^{n_L} V_{drain,i} \cdot V_{g,sfc,i}\,, \tag{30}$$

where n_L is the number of layers, $V_{drain,i}$ is the drainage volume of the i-th layer and $V_{g,sfc,i}$ [v/v_{bulk}] is the volume of hydrocarbon at surface conditions stored in one cubic foot of formation in the *i*th layer.

The AHCIIP can be calculated after every stage of stimulation. To provide estimate of AHCIIP for the whole well with the commonly used three-stage model, we differentiate the first stage from the other stages with consideration of stress shadow effects to the second and third stages but not the first (virgin) stage. Therefore, the accessible hydrocarbon initially in place for the whole well ($AHCIIP_{Well}$) is calculated as:

$$AHCIIP_{Well} = \frac{AHCIIP_{stage3} - AHCIIP_{stage1}}{2} \cdot \left(\frac{l_{well,tot}}{\Delta_{Stage} + l_{Stage}} - 1 \right) + AHCIIP_{stage1}\,, \tag{31}$$

where $l_{well,tot}$ is the total horizontal well length, Δ_{Stage} is the stage spacing and l_{Stage} is the stage length. Note that $AHCIIP_{stage1}$ and $AHCIIP_{stage3}$ are the AHCIIP after Stages 1 and 3 are stimulated. Please note repeatable performance for all stages after Stage 1 is assumed.

Well EUR can be calculated based on $AHCIIP_{Well}$ by assuming a recovery factor. This method fits for assets with limited production data, i.e., appraisal phases. For assets with reasonable amounts of production data, it is recommended to use another approach for EUR calculation. This approach relies on correlating EUR, from production data analysis, such as decline curve analysis, with one of the objective variables from Dynardo simulation, such as TSRV, VSRV, TDV, or AHCIIP. With this correlation, EUR's of wells with different completion designs can be predicted. The two EUR prediction methods can be used to cross check each other for assets with enough production data. UDC prediction can be made using the predicted EUR from a specific completion design and the cost of that completion based on the actual service contracts of the asset.

Sensitivity Study, Parametric Ranking, Meta Model Generation and Optimization

Subsurface parameters are input to the model either as boundary conditions or initial conditions. These parameters have great influences to the objective functions. The impacts of the subsurface parameters on the objective functions depend on their uncertainty ranges as well as their driving mechanisms to hydraulic fracturing. The ranking of the parameters shows which parameter or group of parameters should be focused on in reducing their uncertainties, and thus, provides insight on future data acquisition programs.

The well and completion parameters include well orientation, landing zone, stage and perforation parameters, fluid volume, pumping rate, and fluid viscosity. The current version of the technology does not handle proppant transport, which will be a major update in the upcoming version. The sensitivity study presents a set of well and completion design parameters that define the optimal design to achieve the specific objective defined by the objective function. It also provides the ranking of the well and completion design parameters based on their impacts to the objective functions.

The sensitive study is automatically driven by optiSLang. The optiSLang module searches the uncertainty space defined by the uncertainty ranges of the subsurface as well as well and completion parameters. It comes up with experimental design scenarios, generates ANSYS input files corresponding to the scenarios, launches ANSYS simulations with the input files, takes ANSYS analysis results from the simulations, and saves the scenarios and results in the metamodel. The resulting metamodel is used to rank the input parameters based on their impacts to the objective functions. The ranking is based by the *coefficient of prognosis* (CoP), which is defined as:

$$CoP = 1 - \frac{SS_E^{Prediction}}{SS_T}, \tag{32}$$

where $SS_E^{Prediction}$ is the sum of squared prediction error, $SS_T$is the total variation.

Upon finishing the sensitivity study the metamodels are available inside optiSLang or in Excel. The metamodel provides the opportunity to quickly check scenarios other than that already investigated in the sensitivity study and optimization process. For example, if the optimum completion design from the model showed two clusters were the best cluster design to maximize EUR, one could ask how much EUR reduction would it incur if three or four clusters were used? The metamodel quickly renders an answer. The metamodel also provides the opportunity to handle subsurface parameter changes across different areas of an asset, new well and completion designs, and even changing key business drivers, without building a new model as long as the initial variation windows of reservoir uncertainties and operational parameter covers the design values to be analyzed.

Optimization depends on business drivers. Business drivers can be translated into objective functions as defined in the former sections. The most frequently used objective functions are AHCIIP, EUR and UDC. Maximizing AHCIIP or EUR is to achieve the *technical limit EUR*, which means the maximum achievable EUR if cost for well and completion is not an issue. Because higher hydrocarbon production usually requires higher simulation costs, UDC optimization is to balance EUR versus cost. By plotting EUR's versus costs of different completion designs in a Pareto plot, the optimized design for UDC is obtained. The Pareto frontier of the Pareto plot represents the design limits where production improvement can no longer be achieved without increasing the completion cost. The Pareto frontier is the final result of the Dynardo workflow. It is used for rationalizing the decision between maximizing EUR and minimizing the related completion costs.

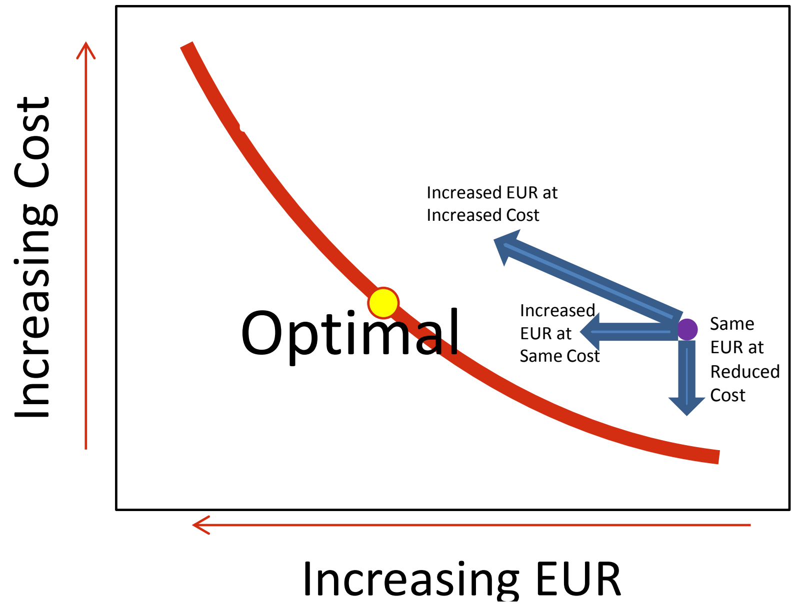

Figure 12: Pareto Plot between EUR and Costs (UDC).

Case Study

After a short period of field development, the standard completion practices in Reservoir X were investigated to improve hydrocarbon production. This was done by applying the Dynardo technology to maximize EUR.

Model Construction, Initialization and Calibration

Figure 12 shows the map view of a well pad in Reservoir X. Well 3-H was chosen as the well to model. It was the first well completed on the pad. Stages 6, 7, and 8 were chosen for the model primarily because of the high quality of microseismic data, which was acquired from a nearby vertical monitoring well, Well 1-V. Also, Stages 6, 7, and 8 were not affected by any faults that might add uncertainties to the modeling results.

Layering of the model was defined based on core and log data derived mechanical properties, lithology types, rock structures and textures, permeability, porosity and hydrocarbon saturation. Thirteen layers were defined in the model (Figure 13). All the three stages were landed in rock layer L04. Based on the layering and geometric measurements of the stages, FEM meshes were constructed as shown in Figure 14.

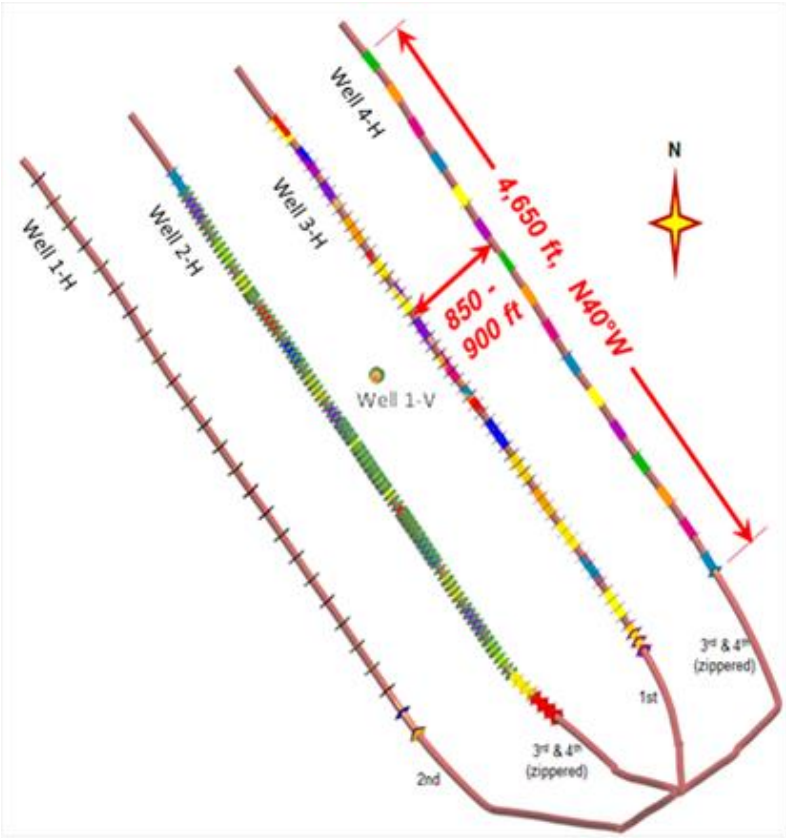

Figure 12: Well Location Map.

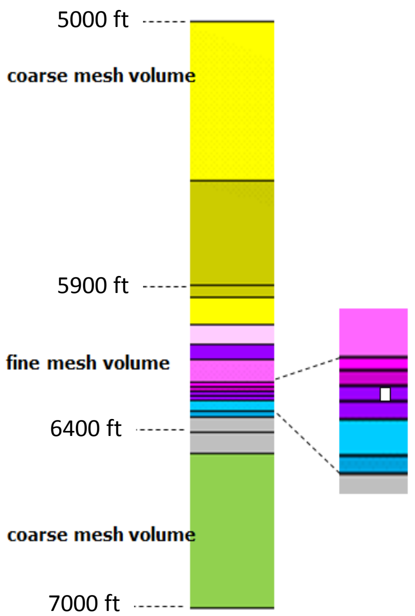

Layer	TVD Top (ft)	TVD Bottom (ft)
L12		5,543
L11	5,543	5,942
L10	5,942	6,034
L09	6,034	6,102
L08	6,102	6,154
L07	6,154	6,231
L06	6,231	6,245
L05	6,245	6,261
L04	6,261	6,294
L03	6,294	6,331
L02	6,331	6,349
L01	6,349	6,474
L00	6,474	

Figure 13: Stratigraphic column of all modeled layers. Please note: Depths are shifted, but the layer thicknesses keep unchanged.

Natural fracture orientations were derived from outcrop fracture mapping and then verified with core data and image log interpretation. Natural fractures and bedding planes were modeled as planes of weaknesses. In addition to the bedding planes, the model considered three sets of planes of weaknesses (Fig. 15) defined by the three sets of vertical natural fractures, which are the first set of vertical natural fractures with dip direction of 135° and dip angle of 80°, the second set of vertical natural fractures with dip direction of 225° and dip angle of 80°, and the third set of vertical natural fractures with dip direction of 175° and dip angle of 80°. A microseismic moment tensor analysis was used to verify shear plane orientations. The microseismic events consistently indicated the activation of the first vertical natural fracture set. The mechanical properties of the intact rocks and the planes of weaknesses were summarized in Table 2.

Initial reservoir pressure was defined for all layers using a pressure gradient of 0.74 psi/ft. Initial in-situ stress field was defined as effective stress for every layer of the reservoir by using a vertical total stress gradient (overburden gradient) of 1.08 psi/ft and conventional relationships between effective vertical stress S_z and effective minimum horizontal stress S_{hmin} (k_0-values) as well as effective maximum horizontal stress S_{Hmax}. Values for k_0 for every layer vary between 0.4 and 0.8. The S_{Hmax} is defined to be an increment of 30% of the difference between S_z and S_{hmin} relative to S_{Hmin}. The direction of maximum horizontal stress direction was defined as being perpendicular to the well direction. Model initialization was conducted to ensure that in-situ stresses, reservoir pressure, rock strengths, and constitutive models do not result in unrealistic plastic deformation.

(a)

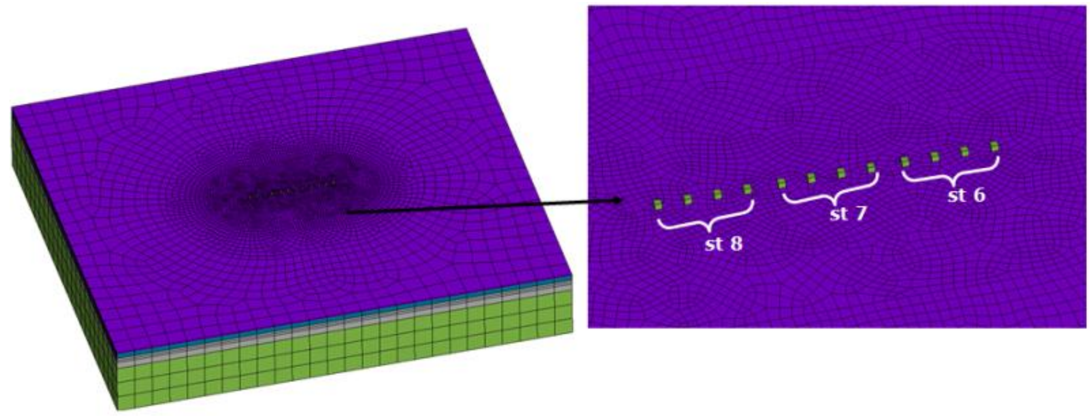

(b)

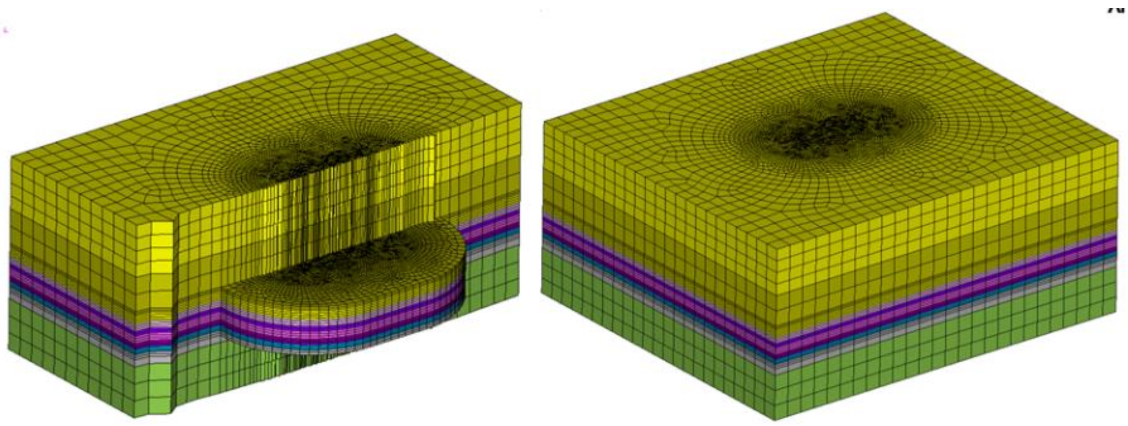

Figure 14: FEM Meshes. (a). FE-Model with stage 6,7,8 and perforations in layer L04. (b). Mesh for hydraulic analysis

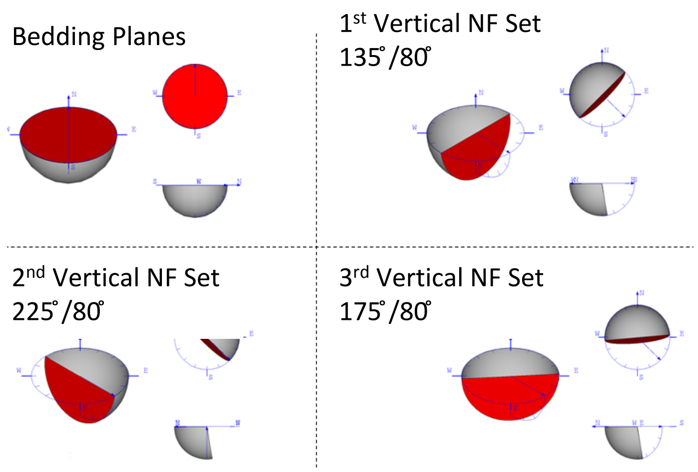

Figure 15: Orientations of the planes of weaknesses considered in the model.

Table 2: Mechanical properties of intact rocks and planes of weaknesses.

	Intact				Bedding plane			1st vertical			2nd vertical			3rd vertical		
	UCS	phi	C	sigt	phi_1	c_1	sigt_1	phi_2	c_2	sigt_2	phi_3	c_3	sigt_3	phi_4	c_4	sigt_4
	[psi]	[°]	[psi]	[psi]	[°]	[psi]	[psi]	[°]	[psi]	[psi]	[°]	[psi]	[psi]	[°]	[psi]	[psi]

L12	14,450	Elastic			Elastic											
L11	19,972	45	4,136	10%	20.44	25	5	20.44	250	50	20.44	250	50	20.44	250	50
L10	21,131	45	4,376	10%	20.44	25	5	20.44	25	5	20.44	125	25	20.44	125	25
L09	17,513	45	3,627	10%	20.44	25	5	20.44	25	5	20.44	125	25	20.44	125	25
L08	17,500	37	4,363	10%	20.44	25	5	no vertical joints			no vertical joints			no vertiacljoints		
L07	17,367	45	3,597	10%	20.44	25	5	20.44	25	5	20.44	125	25	20.44	125	25
L06	16,505	45	3,418	10%	20.44	25	5	20.44	25	5	20.44	125	25	20.44	125	25
L05	16,260	45	3,368	10%	20.44	25	5	20.44	25	5	20.44	125	25	20.44	125	25
L04	15,428	45	3,195	10%	20.44	25	5	20.44	25	5	20.44	125	25	20.44	125	25
L03	9,917	45	2,054	10%	20.44	25	5	20.44	25	5	20.44	125	25	20.44	125	25
L02	11,189	45	2,317	10%	20.44	25	5	20.44	25	5	20.44	125	25	20.44	125	25
L01	29,919	45	6,196	10%	20.44	25	5	no vertical joints			no vertical joints			no vertical joints		
L00	15,145	Elastic			Elastic											

Model calibration was conducted by matching the fracture initiation and termination behaviors from the DFIT data, by matching bottom hole pressure response using pumping rate as input (Fig. 16), and *vice versa* (Fig. 17), by matching the generated fracture volume with the pumped total fluid volume (Fig. 18), and by matching the plastically deformed rocks from the model with the microseismic distributions (Fig. 19).

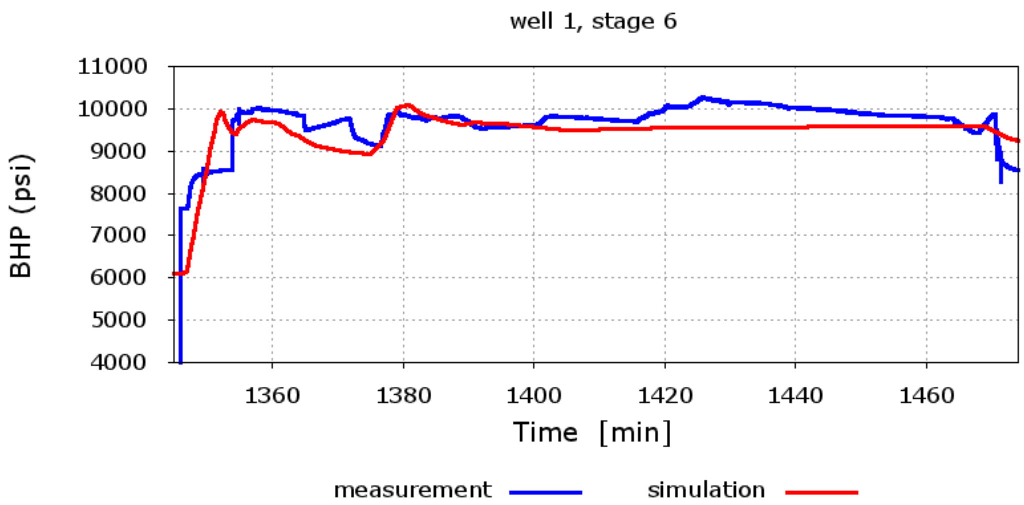

Figure 16: Stage 6 comparison between model calculated BHP (red) versus actual BHP (blue) using pumping rate as input.

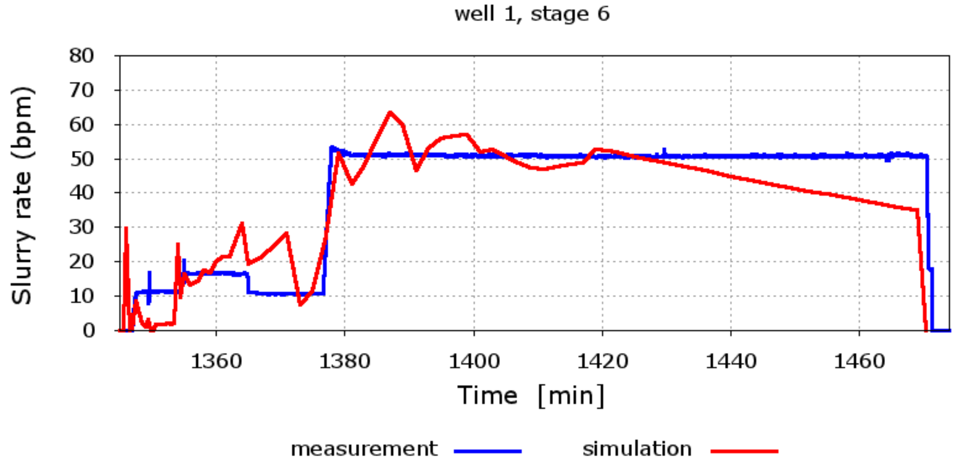

Figure 17: Stage 6 comparison between model calculated pumping rate (red) versus actual pumping rate (blue) using BHP as input.

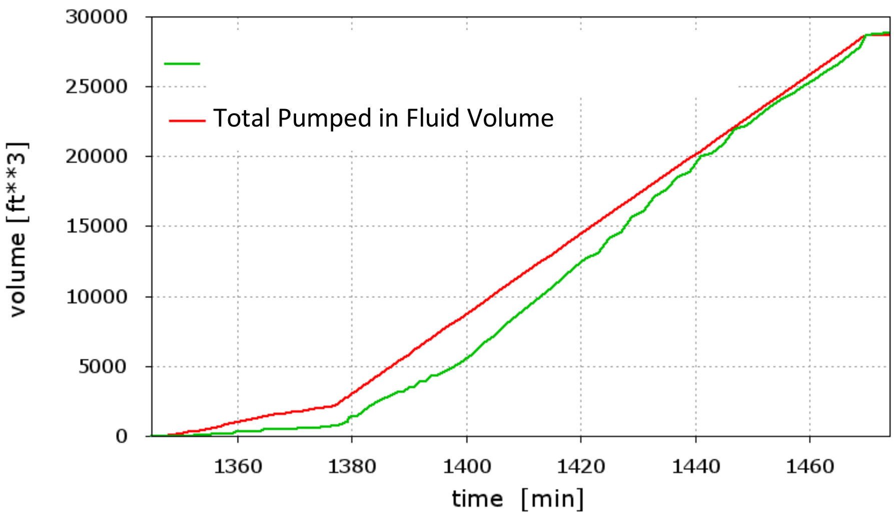

Figure 18: Stage 6 comparison of total pumped in fluid (red) and created connected-water-accepting fracture volume (green).

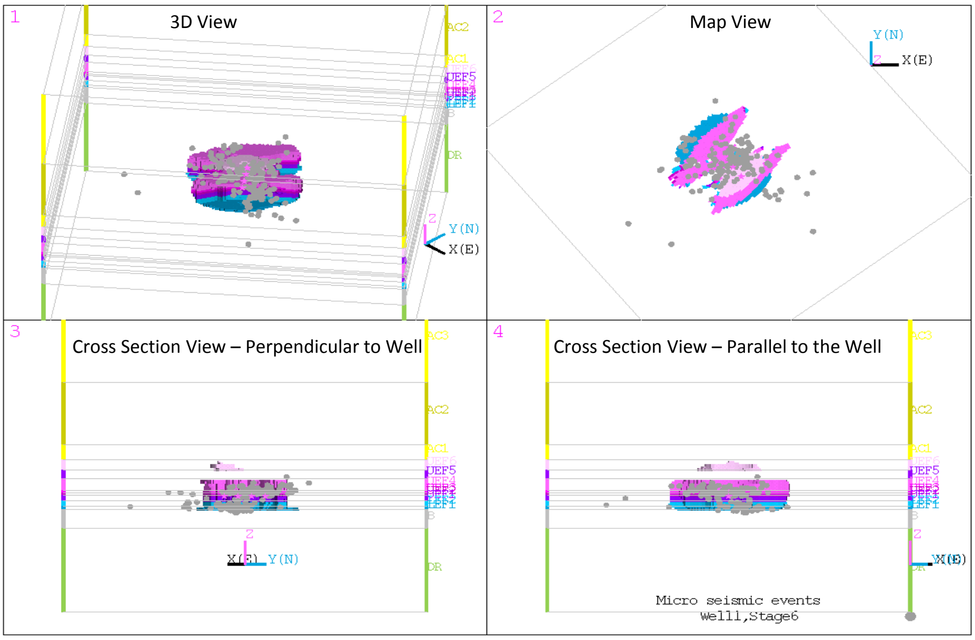

Figure 19: Plot of connected proppant-accepting elements and microseismic events at the end of Stage 6.

Sensitivity Study and Results

The calibrated model was then used to run sensitivity analyses with respect to well and completion design parameters including well landing depth, stage parameters (stage spacing, number of clusters), pumping parameters (pumping rate and volume), and fluid viscosity. The defined uncertainty windows of the parameters are summarized in Table 3. The number of perforations and the well landing depth were defined as discrete parameters. All other parameters continuously varied between the lower and upper bounds. In order to modify pumping rate and total pumped volume using a parametric procedure, the pumping rate function was idealized to be identical for every stage and having identical waiting time between stages.

The objective function was defined as VSRV. To come up with the optimal design with maximized VSRV, the metamodel derived from the sensitivity analysis was used. The optimized design is summarized in Table 3. With the optimized design, potentially doubling of the VSRV was indicated.

Table 3: Well and completion parameters of base design and optimal design and their uncertainty ranges.

Parameter	Reference Design	Uncertainty Range	Optimal Design
Landing Zone (ft)	L04	L02 – L08	L05
Perforation Clusters per Stage	4	1 – 5	1
Stage Spacing (ft)	300	150 – 650	250
Pumping Rate (bpm)	50	30 – 100	100
Total Fluid Volume (bbls)	4500	4000 – 8000	7800

Verification of Model Prediction with Data from Neighboring Wells

The performance of unconventional wells, to a large extent, depends on geology. However, completion is also critical to the success of unconventionals. Because of the large number of uncertain parameters in the process, it is costly to conduct field pilots to understand the impacts of all the parameters. What is proposed here is a physics or model guided approach that enables us to better use available well performance data compared to the commonly applied multi-variant analysis. It reduces the number of field trials needed to come up with optimal completion designs.

To verify the model prediction, we used well completion and performance data of neighboring wells to ensure the wells we compared with were in similar geological settings. The wells were located up to 10,000 feet from the center of the well pad shown in Fig. 12. The EUR numbers were from pressure decline analysis with six months and more production history. The VSRV numbers were from the metamodel built in this study and based on the actual completion parameters of the wells. The EUR's versus VSRV's are plotted in Fig. 21. The plot shows a clear trend of completion impact to well performance. The best fit curve shows a slightly non-liner correlation between EUR and VSRV. It is worth mentioning that the plot was made after the metamodel was built, which means it was a blind prediction.

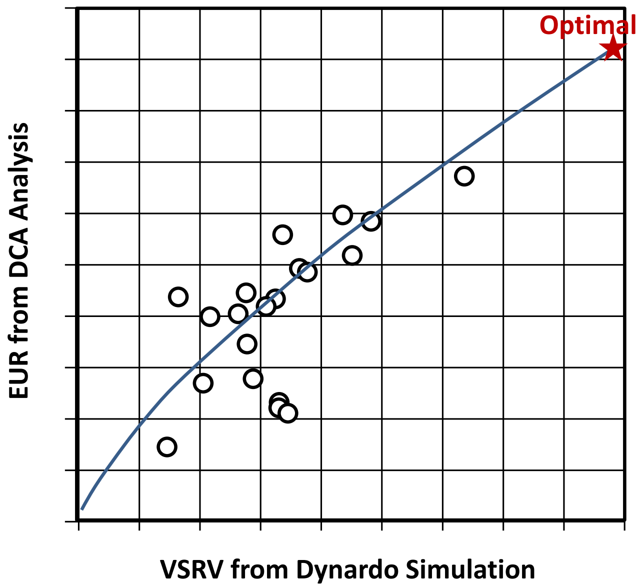

Figure 20: Plot of decline curve analysis (DCA) derived EUR versus Dynardo predicted VSRV values.

Field trials were also conducted to verify the optimal completion design on a five-well pad. Within the five wells, one well was completed with the recommended optimal design based on this work. The other wells were completed with the base completion design of the asset. Early preduction showed more than 20% uplift in production from the well completed with the optimal design compared to the other four wells. Details of the field trials will be explained in another paper.

Summary

The Dynardo technology provides a subsurface based completion optimization toolkit that integrates subsurface, well, completion, production, diagnosis, and cost data for well and asset value delivery.

Compared to common practice, i.e., field trials, the technology offers a much cheaper and faster alternative approach to develop an optimal well completion design for EUR and UDC improvement. Application of the technology clearly showed its predictability. Field trials based on the optimal completion design from Dynardo modeling showed encouraging production uplift. We are convinced that it is feasible to derive an optimal completion design using a subsurface based forward modeling approach that will deliver significant value to the industry.

Acknowledgement

The authors would like to thank Shell Oil Company, especially Bill Westwood, Sam Whitney, Shawn Holzhauser, Simon James, and Lee Stockwell for their continuously supports for Dynardo technology development, case studies and field trials in the past five years. Special thanks to the assets teams in USA, Canada, China, and Argentina for their interests in the technology and for their support for the asset specific studies. Also, thanks to Shawn Holzhauser and Brent Williams for their detailed review of this paper, and to Anna Yankow for editing this paper.

References

Gangi, A. F. (1978). Variation of whole and fractured porous rock permeability with confining pressure. *International Journal of Rock Mechanics and Mining Sciences & Geomechanics Abstracts, 15*(5), 249-257.

ANSYS, Inc. . (2013). *ANSYS ® , Release 14.5* . Canonsburg, PA.

Barton, N., Bandis, S., & Bakhtar, K. (1985, June). Strength, deformation and conductivity coupling of rock joints. *International Journal of Rock Mechanics and Mining Sciences & Geomechanics Abstracts, 22*(3), 121–140.

Bathe, K. J. (1985). *Finite element procedures.* Prentice Hall.

Dynardo GmbH. (2013). *3D Hydraulic fracturing simulator, version 3.7.4, documentation.ppt* . Weimar.

Dynardo GmbH. (2013). *multiPlas – elastoplastic material models for ANSYS, Version 5.0.593.* Weimar.

Dynardo GmbH. (2013). *optiSLang ® - The optimizing Structural Language, Version 4.1.0* . Weimar.

Iragorre, M. T. (2010). *Thermo-hydro-mechanical analysis of joints a theoretical and experimental study.* Barcelona: Phd-Thesis, Univesitat politècnica de Catalunya.

Jirasek, M., & Bazant, Z. P. (2001). *Inelastic Analysis of Structures.* John Wiley & Sons.

Most, T., & Will, J. (2012). Efficient sensitivity analysis for virtual prototyping. *Proceedings of the 6th European Congress on Computational Methods in Applied Sciences and Engineering.* Vienna.

Pölling, R. (2000). *Eine praxisnahe, schädigungsorientierte Materialbeschreibung von Stahlbeton für Strukturanalysen.* Dissertation, Ruhr-Universität Bochum.

Simo, J. C., & Hughes, T. J. (1998). *Computational Inelasticity.* Springer.

Weijers, L. (October 2007). *Evaluation of Oil Industry Stimulation Practices for Engineered Geothermal Systems, Pinnacle Report DOE-PS36-04GO94001.*

Will, J. (1999). Beitrag zur Standsicherheitsberechnung im geklüfteten Fels in der Kontinuums- und Diskontinuumsmechanik unter Verwendung impliziter und expliziter Berechnungsstrategien. In *Berichte des Institutes für Strukturmechanik 2/99.* Dissertation, Bauhaus Universität Weimar.

Will, J., & Schlegel, R. (2010). Simulation of hydraulic fracturing of jointed rock. *Proceedings of European Conference on Fracture.* Dresden.
Wittke, W. (1984). *Felsmechanik: Grundlagen für wirtschaftliches Bauen im Fels.* Springer-Verlag.